Characterizing superradiant dynamics in atomic arrays via a cumulant expansion approach

Oriol Rubies-Bigorda ,[1,2,*,†] Stefan Ostermann ,[2,*,‡] and Susanne F. Yelin[2]

[1]*Physics Department, Massachusetts Institute of Technology, Cambridge, Massachusetts 02139, USA*
[2]*Department of Physics, Harvard University, Cambridge, Massachusetts 02138, USA*

Ordered atomic arrays with subwavelength lattice spacing emit light collectively. For fully inverted atomic arrays, this results in an initial burst of radiation and a fast buildup of coherences between the atoms at initial times. Based on a cumulant expansion of the equations of motion, we derive exact analytical expressions for the emission properties and numerically analyze the full many-body problem resulting in the collective decay process for unprecedented system sizes of up to a few hundred atoms. We benchmark the cumulant expansion approach and show that it correctly captures the cooperative dynamics resulting in superradiance. For fully inverted arrays, this allows us to extract the scaling of the superradiant peak with particle number. For partially excited arrays where no coherences are shared among atoms, we also determine the critical number of excitations required for the emergence of superradiance in one- and two-dimensional geometries. In addition, we study the robustness of superradiance in the case of non-unit filling and position disorder.

I. INTRODUCTION

The interaction of dense atomic ensembles with light gives rise to a plethora of interesting many-body effects. One paradigmatic example is Dicke superradiance [1,2], a phenomenon in which the atoms in a totally inverted pointlike sample synchronize and emit light coherently. This results in the cooperative speedup of the atomic decay process and the emergence of a *superradiant* radiation burst [see Fig. 1(c)]. Various aspects of Dicke superradiance have been studied [3–8] and experimentally observed for a broad variety of platforms, ranging from atomic gases [9–15] to solid-state systems such as quantum dots [16,17], nitrogen-vacancy centers [18], and two-dimensional materials [19].

Over the past few years, ordered atomic arrays with subwavelength lattice spacing have emerged as a promising platform to study collective light-matter coupling in free space. In the few excitation limit, these systems naturally exhibit collective superradiant and subradiant states [20]. Various aspects of this low-excitation regime were studied in detail in recent years [20–31]. However, analyzing the cooperative dynamics for large system sizes in the multiexcitation regime is challenging due to the rapidly growing Hilbert space. This restricts the study of ordered atomic ensembles with multiple excitations to very small systems of about ten

atoms, for which the full solution of the open-system master equation is still feasible by means of Monte Carlo wave function (MCWF) methods [32–34].

For fully inverted atomic ensembles, it has been recently shown that the existence of a superradiant burst can simply be determined from the the statistics of the first two emitted photons [34–37]. This method does not require us to propagate the equations of motion in time, and therefore it enables the efficient analysis of very large systems (up to 10^6 atoms). It provides, however, no information about the decay dynamics, such as the magnitude of the superradiant peak or the existence of subradiance at late times. Alternatively, recent theoretical studies have developed an effective two-atom description of the many-body system capable of capturing superradiance in inverted three- and two-dimensional ensembles [38–40].

In this work, we employ cumulant expansions of the operator expectation values governing the system's dynamics to characterize the decay process of dipole-dipole coupled arrays of atoms [41–44]. Based on neglecting high-order quantum correlations, cumulant or cluster expansions drastically reduce the degrees of freedom used to describe the system. As opposed to MCWF methods [45,46], which require 2^N variables to describe an N-atom array, the cumulant expansion up to order n contains only $\sim N^n$ terms (see the sketch in Fig. 1). To this end, we derive the equations of motion for second- and third-order cumulant expansions in Sec. II, which provide analytical insights into the mechanisms leading to superradiance. We then benchmark the formalism in Sec. III by comparing the resulting dynamics with that predicted by MCWF. We demonstrate that cumulant expansions capture the early dynamics resulting in a superradiant burst with remarkable accuracy, and we find that they allow us to simulate unprecedented system sizes of up to a few hundred atoms, more than one order of magnitude larger than with MCWF.

---

*These authors contributed equally to this work.
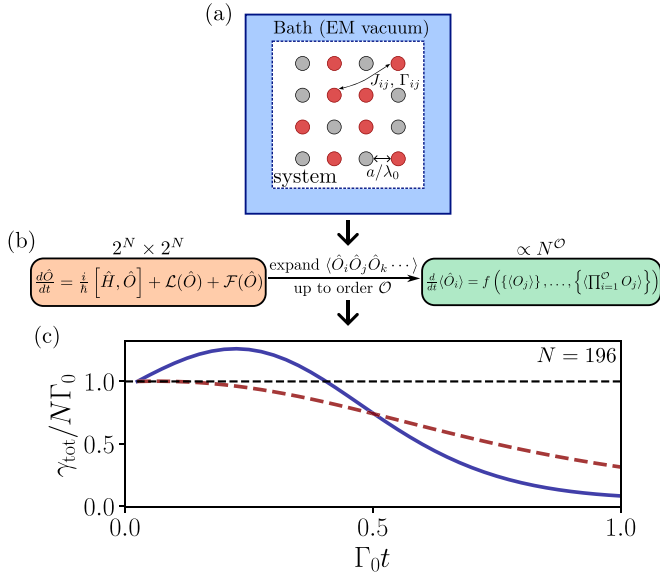
†orubies@mit.edu

‡stefanostermann@g.harvard.edu

FIG. 1. Schematic illustration of the theoretical approach. (a) The EM vacuum mediates interactions among emitters trapped in a periodic array. Superradiant dynamics is characterized for fully or partially excited arrays where no coherences are shared among emitters at $t = 0$. (b) The complexity of the system can be reduced by truncating the number of equations of motion via a cumulant expansion of multiorder correlators. (c) This approach allows the characterization of superradiant dynamics for large system sizes. The bottom panel shows the total emission rate $\gamma_{\rm tot}/(N\Gamma_0)$ for two exemplary time evolutions obtained by numerically solving the equations of motion resulting from a third-order cumulant expansion for a chain of $N = 196$ atoms and two different lattice spacings $a = 0.3\lambda_0$ (solid line) and $a = 0.5\lambda_0$ (dashed line).

Based on these insights, we then employ this formalism to unveil new insights into the physics of superradiant emission (Sec. IV). In particular, we characterize the magnitude of the superradiant peak, and we analyze its scaling as a function of lattice spacing and atom number for large one-dimensional and two-dimensional inverted arrays in Sec. IV A. We additionally demonstrate that the enhanced atomic decay in inverted systems originates from a fast buildup of coherences among atoms. Hence, a natural question arises: what is the critical fraction of excited emitters required for this cooperative synchronization effect to occur if the atoms do not share coherences at initial times? In Sec. IV B, we analytically determine this critical condition for incoherently partially inverted arrays, and further compute the value of the superradiant peak versus excitation fraction using cumulant expansions. Finally, we extend the study to atomic arrays with finite filling fractions in Sec. IV C and with position disorder in Sec. IV D.

II. MODEL

We consider an ensemble of N identical two-level atoms that interact with the vacuum electromagnetic field in free

space. Applying the Markov approximation and integrating out the field degrees of freedom (see Fig. 1), one obtains the equations of motion for the atomic operators in the Heisenberg picture [47,48],

$$\frac{d\hat{O}}{dt} = \frac{i}{\hbar}[\hat{H}, \hat{O}] + \mathcal{L}(\hat{O}) + \mathcal{F}(\hat{O}). \quad (1)$$

Here, $\hat{H}$ and $\mathcal{L}(\hat{O})$, respectively, describe the coherent and incoherent dipole-dipole coupling mediated by the vacuum field,

$$\hat{H} = \sum_{i,j \neq n} J_{ij}\hat{\sigma}_i^{eg}\hat{\sigma}_j^{ge}, \quad (2)$$

$$\mathcal{L}(\hat{O}) = \sum_{i,j} \frac{\Gamma_{ij}}{2}\left(2\hat{\sigma}_i^{eg}\hat{O}\hat{\sigma}_j^{ge} - \hat{\sigma}_i^{eg}\hat{\sigma}_j^{ge}\hat{O} - \hat{O}\hat{\sigma}_i^{eg}\hat{\sigma}_j^{ge}\right), \quad (3)$$

where $\hat{\sigma}_i^{eg} = |e_i\rangle\langle g_i|$ and $\hat{\sigma}_i^{ge} = |g_i\rangle\langle e_i|$ are the raising and lowering operators for atom i, which is located at $\mathbf{r}_i$. Additionally, the coherent J_{ij} and dissipative Γ_{ij} couplings between atoms i and j are obtained from the Green's tensor for a point dipole in vacuum $\mathbf{G}$, given in Appendix A, as

$$J_{ij} - i\Gamma_{ij}/2 = -\frac{3\pi\gamma_0}{\omega_0}\mathbf{d}^\dagger\mathbf{G}(\mathbf{r}_{ij}, \omega_0)\mathbf{d}, \quad (4)$$

where $\omega_0 = 2\pi c/\lambda_0$ corresponds to the transition wavelength of the emitters, $\mathbf{d}$ corresponds to their transition dipole moment, and $\mathbf{r}_{ij} = \mathbf{r}_i - \mathbf{r}_j$ corresponds to the vector connecting atoms i and j. Here, $\Gamma_{ij} = \Gamma_0$ is given by the spontaneous decay rate of a single atom in vacuum, and the Lamb-shift J_{ii} is included in the definition of ω_0. For the remainder of this work, we consider a transition dipole moment perpendicular to the array. Note that similar results are obtained for other polarizations.

Finally, the last term in Eq. (1), $\mathcal{F}(\hat{O})$, describes the quantum Langevin noise arising from vacuum fluctuations [47]. Assuming white noise for $\mathcal{F}(\hat{O})$, the expectation value $\langle\mathcal{F}(\hat{O})\rangle$ vanishes. Since we are ultimately interested in averages over atomic operators $\langle\hat{O}\rangle$, we drop this term in the following discussion to simplify notation.

In this work, we consider initial states where $N_{\rm exc}$ atoms are incoherently excited at $t = 0$,

$$|\psi_{\rm incoh}\rangle = \prod_{i \in E}\hat{\sigma}_i^{eg}|g\rangle, \quad (5)$$

where $|g\rangle$ is the state with all atoms in the ground state, and E denotes the set of initially excited atoms. The two-particle correlations $\langle\hat{\sigma}_i^{eg}\hat{\sigma}_j^{ge}\rangle$ vanish for these states. Hence, no coherences are shared among atoms at initial times even for partially excited arrays. Such states can be prepared by either using a spatially incoherent light source to excite the atomic atomic array or by imposing a random detuning pattern over the duration of the excitation pulse.

The equations of motion of the relevant first- and second-order operators $\hat{\sigma}_i^{ee}$, $\hat{\sigma}_i^{eg}\hat{\sigma}_j^{ge}$, and $\hat{\sigma}_i^{ee}\hat{\sigma}_j^{ee}$ can be readily

obtained from Eq. (1),

$$\frac{d}{dt}\hat{\sigma}_i^{ee} = -\Gamma_0\hat{\sigma}_i^{ee} + \sum_{n\neq i}\left\{\left(iJ_{ni}-\frac{\Gamma_{ni}}{2}\right)\hat{\sigma}_n^{eg}\hat{\sigma}_i^{ge} + \left(-iJ_{in}-\frac{\Gamma_{in}}{2}\right)\hat{\sigma}_i^{eg}\hat{\sigma}_n^{ge}\right\}, \tag{6a}$$

$$\frac{d}{dt}\hat{\sigma}_i^{eg}\hat{\sigma}_j^{ge} = -\Gamma_0\hat{\sigma}_i^{eg}\hat{\sigma}_j^{ge} + \frac{\Gamma_{ji}}{2}\left(4\hat{\sigma}_i^{ee}\hat{\sigma}_j^{ee}-\hat{\sigma}_i^{ee}-\hat{\sigma}_j^{ee}\right) + iJ_{ji}\left(\hat{\sigma}_j^{ee}-\hat{\sigma}_i^{ee}\right)$$
$$+ \sum_{n\neq i,j}\left\{\left(iJ_{jn}+\frac{\Gamma_{jn}}{2}\right)\left(2\hat{\sigma}_j^{ee}\hat{\sigma}_i^{eg}\hat{\sigma}_n^{ge}-\hat{\sigma}_i^{eg}\hat{\sigma}_n^{ge}\right) + \left(-iJ_{ni}+\frac{\Gamma_{ni}}{2}\right)\left(2\hat{\sigma}_i^{ee}\hat{\sigma}_n^{eg}\hat{\sigma}_j^{ge}-\hat{\sigma}_n^{eg}\hat{\sigma}_j^{ge}\right)\right\}, \tag{6b}$$

$$\frac{d}{dt}\hat{\sigma}_i^{ee}\hat{\sigma}_j^{ee} = -2\Gamma_0\hat{\sigma}_i^{ee}\hat{\sigma}_j^{ee} + \sum_{n\neq i,j}\left\{\left(iJ_{nj}-\frac{\Gamma_{nj}}{2}\right)\hat{\sigma}_i^{ee}\hat{\sigma}_n^{eg}\hat{\sigma}_j^{ge} + \left(-iJ_{jn}-\frac{\Gamma_{jn}}{2}\right)\hat{\sigma}_i^{ee}\hat{\sigma}_j^{eg}\hat{\sigma}_n^{ge}\right.$$
$$+ \left(iJ_{ni}-\frac{\Gamma_{ni}}{2}\right)\hat{\sigma}_j^{ee}\hat{\sigma}_n^{eg}\hat{\sigma}_i^{ge} + \left.\left(-iJ_{in}-\frac{\Gamma_{in}}{2}\right)\hat{\sigma}_j^{ee}\hat{\sigma}_i^{eg}\hat{\sigma}_n^{ge}\right\}. \tag{6c}$$

Operators of order n, i.e., involving n products of individual atomic operators, are generally coupled to operators of order $n+1$. This leads to a coupled set of differential equations for system operators up to order N, where N denotes the particle number.

A. Cumulant expansion

The number of equations needed to fully describe the system grows exponentially with atom number, limiting the system sizes that can be numerically simulated to about 16 atoms. To study larger systems, one can take expectation values of the equations of motion in Eq. (6) and truncate the set of equations by approximating averages of higher-order operators with combinations of averages of lower-order ones (see Fig. 1). This method is known as cumulant or cluster expansion [41–44]. For initial states given by Eq. (5), only the three second-order operators given in Eq. (6) develop nonzero expectation values $\langle\hat{\sigma}_i^{ee}\rangle$, $\langle\hat{\sigma}_i^{ee}\hat{\sigma}_i^{ee}\rangle$, $\langle\hat{\sigma}_i^{eg}\hat{\sigma}_j^{ge}\rangle$ during the time evolution. Approximating the three-operator averages in Eq. (6) as $\langle\hat{\sigma}_a^{ee}\hat{\sigma}_b^{eg}\hat{\sigma}_c^{ge}\rangle = \langle\hat{\sigma}_a^{ee}\rangle\langle\hat{\sigma}_b^{eg}\hat{\sigma}_c^{ge}\rangle$, one obtains a closed set of differential equations for the first- and second-order expectation values, which correspond to the second-order cumulant expansion (see Appendix B).

A similar procedure can be used to derive the third-order cumulant expansion of the atomic system, which additionally includes the expectation values $\langle\hat{\sigma}_i^{ee}\hat{\sigma}_j^{ee}\hat{\sigma}_k^{ee}\rangle$ and $\langle\hat{\sigma}_i^{ee}\hat{\sigma}_j^{eg}\hat{\sigma}_k^{ge}\rangle$. The explicit form of the corresponding equations of motion is presented in Appendix C.

B. Emission properties

While a recent theoretical work [44] focused on employing a cumulant expansion approach to determine two-time correlation functions, we focus here on characterizing the emission properties of the atomic array. In fact, the equations of motion corresponding to the second-order cumulant expansion provide a powerful tool to elucidate the fundamental mechanisms resulting in superradiance.

The decay process of the atomic ensemble can be characterized by the excited-state population

$$p_{exc}(t) = \sum_i\langle\hat{\sigma}_i^{ee}\rangle(t) \tag{7}$$

and the total emission rate of the system

$$\gamma_{tot}(t) \equiv -\frac{d}{dt}p_{exc}(t) = \Gamma_0\sum_i\langle\hat{\sigma}_i^{ee}\rangle + \sum_{i,j\neq i}\Gamma_{ij}\langle\hat{\sigma}_i^{eg}\hat{\sigma}_j^{ge}\rangle. \tag{8}$$

Equation (8) provides a very nice intuitive picture on the underlying mechanisms resulting in superradiance. For independent particles ($\Gamma_{ij} = 0$), the emission rate is proportional to the individual atom decay rate Γ_0. For interacting particles, however, the term $\propto \Gamma_{ij}\langle\hat{\sigma}_i^{eg}\hat{\sigma}_j^{ge}\rangle$ modifies the emission rate, and it can eventually result in a superradiant burst if the interactions Γ_{ij} and pair correlations $\langle\hat{\sigma}_i^{eg}\hat{\sigma}_j^{ge}\rangle$ are sufficiently large.

The existence of a radiation burst can be predicted from the derivative of the total emission rate at $t = 0$ [37]. For initial states given by Eq. (5), we obtain

$$\dot{\gamma}_{tot,0} = -\Gamma_0^2\sum_i\langle\hat{\sigma}_i^{ee}\rangle_0 + \sum_{i,j\neq i}\Gamma_{ij}\Gamma_{ji}$$
$$\times\left(2\langle\hat{\sigma}_i^{ee}\hat{\sigma}_j^{ee}\rangle_0 - \frac{\langle\hat{\sigma}_i^{ee}\rangle_0+\langle\hat{\sigma}_j^{ee}\rangle_0}{2}\right), \tag{9}$$

where $\langle\hat{O}\rangle_0 \equiv \langle\hat{O}\rangle(t=0)$. For $\dot{\gamma}_{tot,0} > 0$, the emission rate initially increases, and the dynamics consequently result in a superradiant peak. For $\dot{\gamma}_{tot,0} < 0$, on the other hand, γ_{tot} initially decreases, indicating that the dissipative interactions between emitters cannot build the amount of coherences required for the appearance of a burst. For an initially fully inverted system with $\langle\hat{\sigma}_i^{ee}\rangle_0 = \langle\hat{\sigma}_i^{ee}\hat{\sigma}_j^{ee}\rangle_0 = 1$, Eq. (9) reduces to

$$\dot{\gamma}_{tot,0} = -N\Gamma_0^2 + \sum_{i,j\neq i}\Gamma_{ij}\Gamma_{ji} \tag{10}$$

and is identical to the expressions derived in Ref. [37], as well as to the expression obtained via the two-photon correlation function in Ref. [34]. Note that both Eqs. (9) and (10) are exact, as second-order cumulants perfectly capture two-photon processes at initial times.

While typically sufficient when studying the decay of fully inverted systems or partially excited coherent spin-states [34], this criterion can fail to identify radiation bursts for more general initial conditions. One example is incoherently driven, partially excited arrays, whose initial states are in a
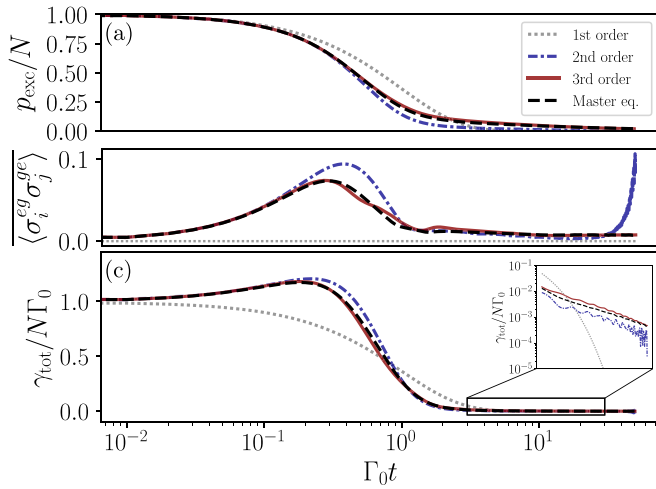
FIG. 2. Comparison between the dynamics obtained via cumulant expansion of orders 1–3 and the solution of the full master equation for a chain of $N = 10$ atoms with lattice spacing $a = 0.1\lambda_0$. (a) Excited-state population $p_{exc}(t)$, (b) average pair correlations, and (c) total emission rate $\gamma_{tot}/(N\Gamma_0)$. The inset in panel (c) represents the total emission rate at late times in logarithmic scale. The atoms are considered to be polarized in the direction perpendicular to the lattice plane throughout this work.

superposition of dark and bright states as it is presented in Ref. [49]. In this case, strong coherent dipole-dipole interactions J_{ij} can generate a net population transfer from subradiant to superradiant states. This phenomenon, which is triggered by the Hamiltonian evolution of the system, only shows signatures in the emission rate for $t > 0$. Consequently, it cannot be captured by Eq. (9), which relies solely on the dissipative couplings and the atomic properties at zero time.

III. BENCHMARKING CUMULANT EXPANSIONS

When simulating the dynamics of coupled spin systems, there is always a tradeoff between the maximum number of particles that can be numerically simulated and the accuracy of the resulting dynamics. Increasing the order of the cumulant expansion, for example, reduces the former and generally improves the latter. In this section, we study which expansion order is required to correctly capture the evolution of the atomic ensemble. This analysis can only be performed for small system sizes, for which a full solution of the master equation is possible.

In Fig. 2, we plot the dynamic properties of a fully inverted ten-atom chain with lattice spacing $a = 0.1\lambda_0$ using first-order (gray dotted line), second-order (blue dash-dotted line), and third-order (red solid line) cumulant expansions, as well as the solution of the full master equation (black dashed). Third-order cumulants exhibit very good agreement with the exact time evolution and properly capture the magnitude of the superradiant peak (maximum of γ_{tot}/N), while second-order cumulants slightly overestimate it. The outburst of radiation is accompanied by a buildup of the atomic coherences $\langle \hat{\sigma}_i^{eg} \hat{\sigma}_j^{ge} \rangle$ at early times due to the repeated application of the same bright jump operators [34]. At late times, however, the performance of the cumulant expansion worsens. In particular, the second-order cumulant expansion fails to correctly predict
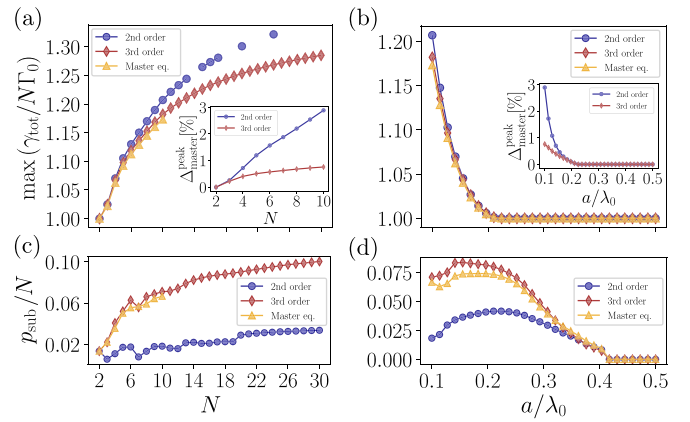

FIG. 3. Benchmarking the cumulant expansion method. (a) Maximum value of the superradiant peak for a fully inverted chain of atoms with lattice spacing $a = 0.1\lambda_0$ as a function of atom number. (b) Value of the superradiant peak for an $N = 10$ atom chain as a function of lattice spacing. The insets in panels (a) and (b) show the relative error between the exact master equation solution and the cumulant expansions in percent. (c),(d) Magnitude of the subradiant population p_{sub}, i.e.,the excited population left in the array by the time the instantaneous decay rate $\gamma_{inst} = \gamma_{tot}/(p_{exc}\Gamma_0) = 0.1$, as a function of (c) particle number and (d) lattice spacing. Same parameters as in panels (a) and (b).

the late dynamics [see the inset in Fig. 2(c)], and the third-order cumulant expansion sometimes results in unphysical behaviors such as growing excitation number in the absence of drive [44]. This poor performance at late times can be attributed to the population of subradiant states during the decay process. These states are typically highly entangled, and therefore contain many high-order inter-atom coherences that lead to destructive interference of the electromagnetic field emitted by different atoms. Consequently, an expansion that neglects higher-order coherences performs worse in predicting these quantities. For very large system sizes ($N > 100$) and small lattice spacings, the cumulant expansion can also result in unphysical behaviors such as a growing excited-state population in the absence of drive.

Finally, it is worth noting that the first-order cumulant expansion, commonly referred to as the mean-field approximation, simply results in an independent exponential decay of the atomic ensemble (without a buildup of the atomic coherences) and does not capture either super- or subradiance.

To benchmark the accuracy of cumulant expansions of different orders, we compare two figures of merit of the decay of inverted atomic arrays as a function of particle number N and lattice spacing a. In Fig. 3(a), we plot the maximum emission rate or magnitude of the superradiant peak, $\max(\gamma_{tot}/N)$, as a function of particle number N for a one-dimensional chain with lattice spacing $a = 0.1\lambda_0$. The inset shows the error made by second-order (blue circles) and third-order (red diamonds) cumulant expansions, defined as $\Delta_{master}^{peak} = \max(\gamma_{tot}^{cum})/\max(\gamma_{tot}^{master}) - 1$, in percent. Not surprisingly, third-order cumulant expansions are more accurate than second-order ones and, more importantly, their error does *not* grow linearly with N. Figure 3(b) demonstrates that the accuracy worsens considerably with decreasing lattice spacing.

This effect can be attributed to the rapidly growing energy shifts, which generate correlations between atoms.

Another relevant quantity that characterizes the decay process of the ensemble is the subradiant population p_{sub}, that is, the amount of excitation left in the atomic array once the system enters the subradiant regime. This occurs once the instantaneous decay rate $\gamma_{inst} \equiv \gamma_{tot}/(p_{exc}\Gamma_0)$ goes below 0.1, as defined in Ref. [49]. Again, third-order cumulants provide an excellent estimate of this quantity, while second-order cumulants fail to capture it. The larger errors of second-order cumulants when estimating p_{sub} as opposed to $\max(\gamma_{tot}/N)$ are due to the fact that the former contains information of the decay process until times much longer than the radiation burst, where subradiant evolution starts to dominate. Still, p_{sub} largely depends on the superradiant dynamics and is therefore accurately captured by the third-order cumulant expansions [49], even if the subsequent subradiant evolution is not [see the inset of Fig. 2(c)].

IV. SUPERRADIANCE

Having elucidated the accuracy with which second- and third-order cumulant expansions capture superradiance, we now investigate the conditions under which this phenomenon emerges in one- and two-dimensional atomic arrays, as well as the magnitude of the radiation burst reached by the ensemble of emitters.

A. Fully inverted arrays

Superradiant emission is typically studied in fully inverted arrays, where all atoms have been initially excited by an intense laser drive. In this scenario, the existence of a burst as a function of system size and lattice spacing can be inferred from Eq. (10) [34–37]. This condition is only based on the structure of the equations of motion at $t = 0$, and no predictions on the resultant time evolution can be made. Here, we use the cumulant expansions approach outlined above to extend previous studies [34–37,39,40,44] on superradiance in ordered subwavelength arrays by analyzing the time evolution leading to superradiance. This allows us to quantify the magnitude of the superradiant peak for system sizes of a few hundred atoms, compatible with state-of-the-art experiments.

In Fig. 4 we determine the superradiant regime for different particle numbers and lattice spacings for a chain of atoms [Fig. 4(a)] and a square lattice [Fig. 4(b)]. We calculate the time evolution for a certain set of parameters (N and a) by solving the cumulant equations up to second order, and we determine the maximum of the total emission rate, which is plotted as a color code in Figs. 4(a) and 4(b). A superradiant peak occurs if $\max(\gamma_{tot}) > N\gamma_0$, that is, if the maximum emission rate is larger than that of independent decay. The white solid line separates the regime where a superradiant burst occurs from the regime where no cooperative enhancement of the atomic emission takes place, and it coincides with the critical value obtained from Eq. (10). The results presented in Figs. 4(a) and 4(b) demonstrate that the transition between both regimes is not sharp, and they suggest that lattice spacings well below the ones predicted in Refs. [34–37] [white lines in Figs. 4(a) and 4(b)] are required to experimentally observe the initial speedup of radiation.
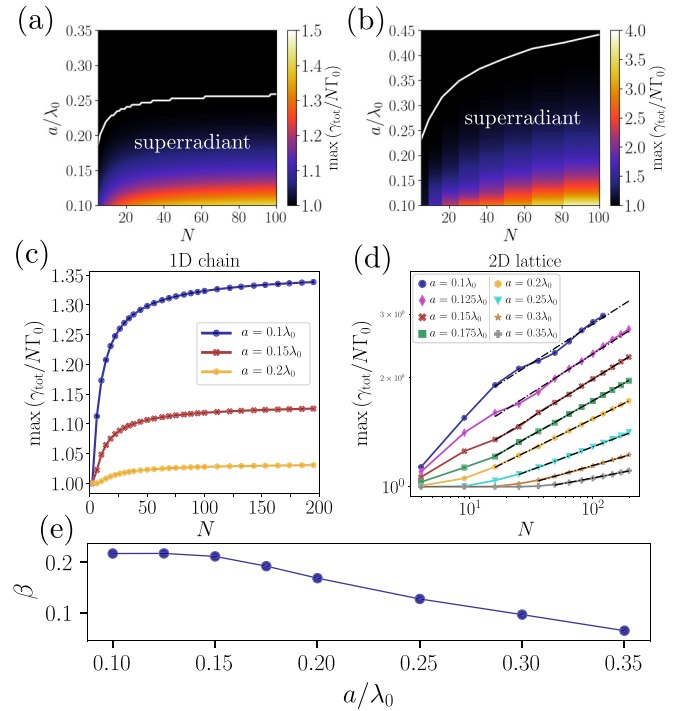

FIG. 4. (a),(b) Maximum emission rate $\max(\gamma_{tot}/N\Gamma_0)$ for (a) an atomic chain and (b) a two-dimensional square lattice as a function of particle number N and spacing a/λ_0 obtained via a second-order cumulant expansion. The white solid line separates the region where a superradiant burst is observed from the region where no superradiance occurs. (c),(d) Scaling of the superradiant peak as a function of particle number for (c) a chain and (d) a square lattice for different lattice spacings. (e) Exponent β characterizing the power-law dependence of the superradiant peak with particle number, $\propto N^\beta$, for a square lattice. The values are obtained from the linear fits in panel (d), shown as dash-dotted lines.

Figures 4(c) and 4(d) show the scaling of the superradiant peak with particle number for a 1D chain and a square lattice, respectively (obtained with a third-order cumulant expansion). We find that the maximum emission rate saturates for $N \to \infty$ for a one-dimensional chain, whereas it increases as $\propto N^\beta$ for a two-dimensional configuration. Performing linear fits of the curves shown in Fig. 4(d), we find that the exponent β increases for decreasing lattice spacing until it saturates for $a/\lambda_0 \to 0$ [see Fig. 4(e)]. It is worth noting that the values of β found in this work are consistent with those reported in Ref. [39].

B. Partially inverted arrays

For fully inverted arrays, the mechanism resulting in superradiance relies on the fast buildup of coherences between pairs of atoms [see Eq. (8) and Fig. 2(b)]. The natural question arises: how many atoms need to be excited for these coherences to build up fast enough and for a superradiant burst to occur? For that, we consider atomic ensembles driven by an incoherent driving field, such that only N_{exc} randomly selected emitters are excited. This type of initial state, where $\langle \hat{\sigma}_i^{eg} \hat{\sigma}_j^{ge} \rangle_0 = 0$, can be generally described by Eq. (5). In the inset of Fig. 5(a), we show in gray the emission rate for
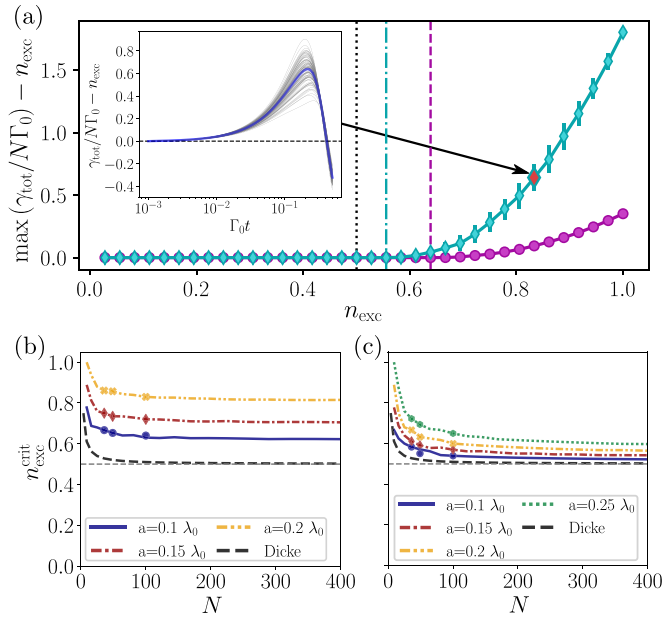
FIG. 5. (a) Value of the superradiant peak as a function of the initial incoherent excitation fraction for $N = 36$ atoms. Magenta diamonds correspond to a one-dimensional chain and cyan diamonds to a two-dimensional square lattice, both with spacing $a/\lambda_0 = 0.1$. The inset shows the time evolution of 100 trajectories, each of them corresponding to a different, random initial distribution of 30 excitations. The blue curve indicates the average over all trajectories and is used to determine the magnitude of the superradiant peak shown in the main figure. The vertical dashed and dash-dotted lines correspond to the critical excitation fraction, determined by Eq. (12) for atomic chains and two-dimensional lattices, respectively. (b),(c) Critical excitation, obtained via Eq. (12), as a function of particle number for (b) one-dimensional and (c) two-dimensional arrays with different lattice spacings. For $a/\lambda_0 \to 0$ the system approaches the Dicke case (black dashed line). The blue circles ($a/\lambda_0 = 0.1$), red diamonds ($a/\lambda_0 = 0.15$), yellow crosses ($a/\lambda_0 = 0.2$), and green hexagons ($a/\lambda_0 = 0.25$) are obtained numerically and show a good agreement with the analytical result.

different initialization of a square lattice with 36 atoms, 30 of which are initially excited. While the exact magnitude of the burst depends on the specific configuration of excited atoms, one can extract a characteristic peak size by averaging over all trajectories (thick blue line). The resulting average peak size is then plotted as a function of the fraction of excited atoms, $n_{\text{exc}} := N_{\text{exc}}/N$, in Fig. 5(a). We find that there is a critical excitation fraction, $n_{\text{exc}}^{\text{crit}}$, required to obtain a superradiant burst both for atomic chains and two-dimensional arrays, which depends both on system size and the specific geometry.

One can analytically compute $n_{\text{exc}}^{\text{crit}}$ by averaging Eq. (9) over all possible configurations of excited atoms. Defining $N_{\text{de}} = N - N_{\text{exc}}$ as the number of deexcited atoms, we obtain an average derivative of the emission rate at $t = 0$ equal to (for details, see Appendix D)

$$\bar{\gamma}_{\text{tot},0} = -N_{\text{exc}}\Gamma_0^2 + \left(1 - \frac{3N_{\text{de}}}{N} + \frac{2N_{\text{de}}(N_{\text{de}} - 1)}{N(N-1)}\right)$$
$$\times \sum_{n,m\neq n} \Gamma_{ij}\Gamma_{ji}. \quad (11)$$

A superradiant burst is observed for $\bar{\gamma}_{\text{tot},0} > 0$, that is, for

$$n_{\text{exc}} > \frac{1}{2} + \frac{1}{2N} + \frac{N-1}{2\sum_{n,m\neq n}\Gamma_{ij}\Gamma_{ji}/\Gamma_0^2}. \quad (12)$$

This analytical result shows perfect agreement with the numerically obtained results [see the vertical dashed and dash-dotted lines in Fig. 5(a)].

In the Dicke limit $a \to 0$, where all emitters are located at the same spatial position, all dissipative couplings are equal to the spontaneous decay rate, i.e., $\Gamma_{mn} = \Gamma_0 \, \forall m, n$, and Eq. (12) results in $n_{\text{exc}}^{\text{crit}} = 1/2 + 1/N$. That is, an excitation fraction larger than one-half, i.e., $N_{\text{exc}} > N/2 + 1$, is required to observe a burst. This can be intuitively understood by realizing that the symmetric Dicke state with maximum decay rate corresponds to the state where half of the atoms are excited. Hence, an initially fully inverted system dynamically evolves into states with higher and higher decay rates while cascading down the Dicke ladder, which ultimately results in the appearance of a superradiant emission peak. Once half of the atoms are deexcited, this trend reverses and the system starts populating states with decreasing decay rates, causing the peak to vanish. If only half (or less) of the atoms are excited initially, the system will never decay into states with a larger decay rate than the initial one, and the atomic ensemble is bound to decay exponentially without the emergence of a burst.

The analytical result in Eq. (12) provides insight into the role of the lattice geometry and dimensionality for arbitrary system sizes. For extended arrays of arbitrary dimension, the sum in the denominator of Eq. (12) is always smaller than for the Dicke case, and a larger excitation fraction is needed to attain superradiance. In one-dimensional arrays, the critical excitation fraction tends to a constant for large particle number, as shown in Fig. 5(b). In two-dimensional arrays [see Fig. 5(c)], however, it decays logarithmically with system size N, $\lim_{N\to\infty} n_{\text{exc}}^{\text{crit}}/N \sim 1/2 + A/\ln(\sqrt{N})$, and eventually reaches the Dicke limit for infinite systems. For completeness, it can be shown that this scaling is improved in three-dimensional lattices, where $\lim_{N\to\infty} n_{\text{exc}}^{\text{crit}}/N \sim 1/2 + A \times N^{-1/3}$ [36,37]. Figures 5(b) and 5(c) also show that a larger excitation fraction is needed to attain superradiance in atomic chains than in a square lattice for equal atom number N and lattice spacing a, as well as the fact that smaller values of a result in a smaller $n_{\text{exc}}^{\text{crit}}$.

Hence, Fig. 5 and Eq. (12) show that there exists a well-defined critical light intensity of the excitation pulse for which superradiance emerges. It is worth noting, however, that Eq. (12) can fail to identify superradiant bursts triggered by the Hamiltonian dynamics at times later than $t = 0$ (for details, see Refs. [38,49]). While these may result in superradiant peaks appearing for $n_{\text{exc}} < 0.5$, they require strong coherent couplings J_{ij} or large dephasing or Doppler broadening and therefore do not typically appear for lattice spacings $a \geqslant 0.1\lambda_0$ considered in Fig. 5.

Finally, it is worth noting that, in experimental implementations of superradiance, the excitation pulse might not be able to fully invert the atom system. Our results show that superradiance is reasonably robust to finite excitation fraction, as a
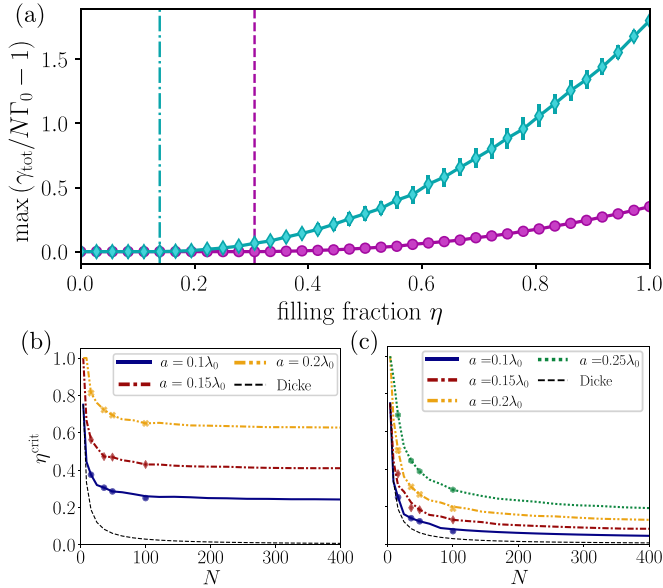
FIG. 6. (a) Value of the superradiant peak for finite filling fractions η for a fully inverted array. Magenta diamonds correspond to a one-dimensional chain and cyan diamonds to a two-dimensional square lattice, both with spacing $a/\lambda_0 = 0.1$. (b),(c) Critical filling fraction to observe a superradiant peak, obtained via Eq. (14), as a function of particle number for (b) one-dimensional and (c) two-dimensional arrays with different lattice spacings. For $a/\lambda_0 \to 0$, the system approaches the Dicke case (black dashed line). The blue circles ($a/\lambda_0 = 0.1$), red diamonds ($a/\lambda_0 = 0.15$), yellow crosses ($a/\lambda_0 = 0.2$), and green hexagons ($a/\lambda_0 = 0.25$) are obtained numerically and show a good agreement with the analytical result.

radiation outburst still occurs at low enough lattice spacings even if only 90% or less of the atoms are initially excited.

C. Finite filling fractions

Typically, experimental implementations of atomic arrays also suffer from a finite filling fraction of the lattice. In Ref. [21], for example, which demonstrated that a two-dimensional array with subwavelength spacing can reflect incident beams of low intensities, approximate filling fractions of 90% were achieved. Here, we show that superradiance for fully inverted arrays is very robust to missing atoms and that large superradiant bursts can still be achieved for filling fractions much lower than those attainable in state-of-the-art experiments.

Figure 6(a) shows a similar analysis to that performed in the previous section. Now, however, that all atoms are initially excited and only a fraction $\eta \equiv N_{\text{filled}}/N$ of the N available lattice sites is populated by an excited atom. In other words, the lattice contains $N_{\text{hol}} = N - N_{\text{filled}}$ holes or missing atoms. Figure 6 shows the average magnitude of the peak for one- and two-dimensional arrays with $N = 36$ lattice sites as a function of the filling fraction η. The peak values are again obtained by averaging over time evolutions for 100 random distributions of holes. The magnitude of the peak slowly decreases with diminishing η, and finally reaches zero at a critical filling fraction $\tilde{n}_{\text{exc}}^{\text{crit}}$ that depends on the properties of the atomic ensemble.

Again, we can estimate η^{crit} by averaging $\dot{\gamma}_0$ over all possible configurations of missing atoms (for details, see Appendix E)

$$\bar{\dot{\gamma}}_{\text{tot},0} = -N_{\text{filled}}\Gamma_0^2 + \left(1 - \frac{2N_{\text{hol}}}{N} + \frac{N_{\text{hol}}(N_{\text{hol}} - 1)}{N(N - 1)}\right)$$
$$\times \sum_{i,j\neq i} \Gamma_{ij}\Gamma_{ji}. \tag{13}$$

On average, a burst occurs for $\bar{\dot{\gamma}}_{\text{tot},0} > 0$, that is, for

$$\eta > \frac{1}{N} + \frac{N - 1}{\sum_{i,j\neq i}\Gamma_{ij}\Gamma_{ij}/\Gamma_0^2}. \tag{14}$$

In the Dicke limit, Eq. (14) reduces to the well-known expression $\eta > 2/N$, i.e., $N_{\text{filled}} > 2$. For two atoms, the decay rates from $|ee\rangle$ to $(|eg\rangle + |ge\rangle)/\sqrt{2}$ and from $(|eg\rangle + |ge\rangle)/\sqrt{2}$ to $|gg\rangle$ are both $2\Gamma_0$. The two-atom system therefore decays faster than in vacuum, but it cannot develop a superradiant burst. For this to occur, the system needs to dynamically access states with larger and larger decay rates while cascading down the Dicke ladder, which naturally occurs for ensembles with three or more atoms. Additionally, it is straightforward to check that $n_{\text{exc}}^{\text{crit}} = 1/2 + \eta^{\text{crit}}/2$. Thus, the scalings presented in Sec. IV B also hold for the case of missing atoms.

It is worth noting that the excitation fraction needed to observe a peak is considerably larger in the case of partially excited configurations, presented in Sec. IV B, than in the case of missing atoms or holes. The main difference between both scenarios consists in the fact that the latter remains a fully inverted system while the former does not. That is, an inverted array with missing atoms can simply cascade down the whole ladder of superradiant states by repeated action of the brightest jump operator—which is now weaker than in a perfect array—and can therefore attain a burst even for very small filling fractions. However, this is not the case for incoherent partially inverted arrays, whose initial state is already a superposition of bright and dark states in an intermediate sector of the state space (see also Ref. [49]) and therefore has a reduced likelihood to quickly build up the necessary correlations to create a superradiant burst.

D. Position disorder

Another potential imperfection that might influence the superradiant burst in realistic setups is disorder in the atomic positions. This can either be due to some distortion in the underlying trapping potential or due to atomic motion in the respective trapping potentials.

To take position disorder into account, we sample the modified atomic positions from a normal distribution $\mathcal{N}_d(\mathbf{r}_0, \sigma)$, where σ denotes its standard deviation and $\mathbf{r}_0$ denotes the positions of the disorderless array. We then average over 100 different excitation and disorder patterns and plot the determined peak height in Fig. 7. We find that the effect of disorder remains small as long as σ is below $0.1a/\lambda_0$, but rapidly increases for larger σ (see the green curves in Fig. 7). Still, these results suggest that superradiance is very robust against position disorder.
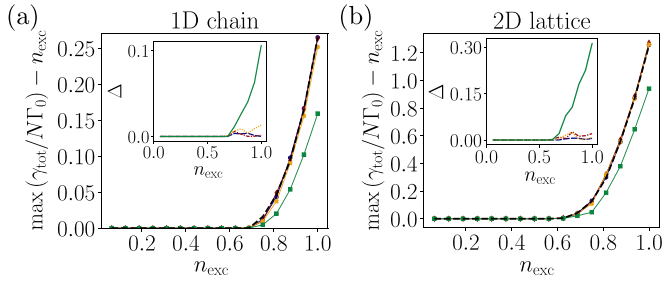
FIG. 7. Effect of position disorder, sampled from a Gaussian distribution with standard deviation $\sigma = (0.01, 0.05, 0.1, 0.2)a$ (blue circles, red diamonds, orange crosses, green squares) for a chain (a) and a square lattice (b) of $N = 16$ atoms and averaged over 50 different lattice configurations and initial excitation distributions. The dashed lines show the result for a perfect lattice without position disorder. The insets exhibit the difference $\Delta = \max\{\gamma_{\text{tot}}/(N\Gamma_0)\}|_{\sigma=0} - \max\{\gamma_{\text{tot}}/(N\Gamma_0)\}|_{\sigma}$ between the zero disorder case and the disordered systems. Disorder affects superradiance if $\sigma > 0.1a$.

V. CONCLUSIONS

We performed a numerical and analytical in-depth analysis of superradiance in ordered atomic arrays based on a cumulant expansion approach. This formalism captures with remarkable accuracy the early-time dynamics where the level of entanglement between atoms is sufficiently small. This allowed us to simulate the open system dynamics of dipole-dipole coupled quantum emitters for reasonably large particle numbers, and to gain insights into the physics behind super- and subradiance. In particular, we identify the scaling of the superradiant peak with particle number both for one-dimensional and two-dimensional arrays. Additionally, we show that there exists a critical excitation fraction above which a superradiant burst occurs, and we demonstrate that superradiance is a robust phenomenon that prevails in the presence of position disorder and finite filling and excitation fraction.

The results presented here are expected to be readily observable in various state-of-the-art platforms, ranging from atomic tweezers [50] and optical lattices of cold atoms [21] to solid-state platforms such as two-dimensional materials [19,51] or vacancy centers in crystals [18]. Our work also paves the way towards efficiently calculating dynamic light emission patterns from atomic arrays, as well as towards devising novel schemes to prepare multiexcitation subradi-

ant states [49]. Finally, the existence of a critical excitation fraction to attain superradiance exhibits a certain resemblance with the superradiant transition in the driven dissipative Dicke model [52–55]. Exploring this connection is an exiting avenue for future work.

APPENDIX A: GREEN'S FUNCTION

The Green's function for a point dipole in free space used in Eq. (4) can be written in Cartesian coordinates as [56,57]

$$G_{\alpha\beta}(\mathbf{r}, \omega) = \frac{e^{ikr}}{4\pi r}\left[\left(1 + \frac{i}{kr} - \frac{1}{(kr)^2}\right)\delta_{\alpha\beta} \right.$$
$$\left. + \left(-1 - \frac{3i}{kr} + \frac{3}{(kr)^2}\right)\frac{r_\alpha r_\beta}{r^2}\right] + \frac{\delta_{\alpha\beta}\delta^{(3)}(\mathbf{r})}{3k^2},$$
$$\tag{A1}$$

where $k = \omega/c$, $r = |\mathbf{r}|$, and $\alpha, \beta = x, y, z$.

APPENDIX B: SECOND-ORDER CUMULANT EXPANSION

For initial states with no correlations as defined in Eq. (5), the only nonzero expectation values of first- and second-order operators at $t = 0$ are

$$\langle\hat{\sigma}_i^{ee}\rangle(t = 0) = \begin{cases} 1 & \text{if atom } i \text{ is excited,} \\ 0 & \text{otherwise;} \end{cases} \tag{B1a}$$

$$\langle\hat{\sigma}_i^{ee}\hat{\sigma}_j^{ee}\rangle(t = 0) = \begin{cases} 1 & \text{if atom } i \text{ and } j \text{ are excited,} \\ 0 & \text{otherwise.} \end{cases} \tag{B1b}$$

Using Eq. (1), one can show that the only additional expectation values that become nonzero during the evolution of the system are $\langle\hat{\sigma}_i^{eg}\hat{\sigma}_j^{ge}\rangle$. This confirms that Eq. (6) is sufficient to describe the dynamics of the atomic ensemble up to second order.

Taking expectation values in Eq. (6) and replacing averages over third-order operators by [41,43]

$$\langle\hat{O}_1\hat{O}_2\hat{O}_3\rangle = \langle\hat{O}_1\rangle\langle\hat{O}_2\hat{O}_3\rangle + \langle\hat{O}_2\rangle\langle\hat{O}_1\hat{O}_3\rangle + \langle\hat{O}_3\rangle\langle\hat{O}_1\hat{O}_2\rangle - 2\langle\hat{O}_1\rangle\langle\hat{O}_2\rangle\langle\hat{O}_3\rangle, \tag{B2}$$

one obtains a closed set of differential equations for the second-order cumulants

$$\frac{d}{dt}\langle\hat{\sigma}_i^{ee}\rangle = -\Gamma_0\langle\hat{\sigma}_i^{ee}\rangle + \sum_{n\neq i}\left\{\left(iJ_{ni} - \frac{\Gamma_{ni}}{2}\right)\langle\hat{\sigma}_n^{eg}\hat{\sigma}_i^{ge}\rangle + \left(-iJ_{in} - \frac{\Gamma_{in}}{2}\right)\langle\hat{\sigma}_i^{eg}\hat{\sigma}_n^{ge}\rangle\right\}, \tag{B3a}$$

$$\frac{d}{dt}\langle\hat{\sigma}_i^{eg}\hat{\sigma}_j^{ge}\rangle = -\Gamma_0\langle\hat{\sigma}_i^{eg}\hat{\sigma}_j^{ge}\rangle + \frac{\Gamma_{ji}}{2}\left(4\langle\hat{\sigma}_i^{ee}\hat{\sigma}_j^{ee}\rangle - \langle\hat{\sigma}_i^{ee}\rangle - \langle\hat{\sigma}_j^{ee}\rangle\right) + iJ_{ji}\left(\langle\hat{\sigma}_j^{ee}\rangle - \langle\hat{\sigma}_i^{ee}\rangle\right)$$
$$+ \sum_{n\neq i,j}\left\{\left(iJ_{jn} + \frac{\Gamma_{jn}}{2}\right)\langle\hat{\sigma}_i^{eg}\hat{\sigma}_n^{ge}\rangle(2\langle\hat{\sigma}_j^{ee}\rangle - 1) + \left(-iJ_{ni} + \frac{\Gamma_{ni}}{2}\right)\langle\hat{\sigma}_n^{eg}\hat{\sigma}_j^{ge}\rangle(2\langle\hat{\sigma}_i^{ee}\rangle - 1)\right\}, \tag{B3b}$$

$$\frac{d}{dt}\langle\hat{\sigma}_i^{ee}\hat{\sigma}_j^{ee}\rangle = -2\Gamma_0\langle\hat{\sigma}_i^{ee}\hat{\sigma}_j^{ee}\rangle + \sum_{n\neq i,j}\left\{\left(iJ_{nj}-\frac{\Gamma_{nj}}{2}\right)\langle\hat{\sigma}_i^{ee}\rangle\langle\hat{\sigma}_n^{eg}\hat{\sigma}_j^{ge}\rangle + \left(-iJ_{jn}-\frac{\Gamma_{jn}}{2}\right)\langle\hat{\sigma}_i^{ee}\rangle\langle\hat{\sigma}_j^{eg}\hat{\sigma}_n^{ge}\rangle\right.$$

$$\left.+\left(iJ_{ni}-\frac{\Gamma_{ni}}{2}\right)\langle\hat{\sigma}_j^{ee}\rangle\langle\hat{\sigma}_n^{eg}\hat{\sigma}_i^{ge}\rangle + \left(-iJ_{in}-\frac{\Gamma_{in}}{2}\right)\langle\hat{\sigma}_j^{ee}\rangle\langle\hat{\sigma}_i^{eg}\hat{\sigma}_n^{ge}\rangle\right\}. \tag{B3c}$$

APPENDIX C: THIRD-ORDER CUMULANT EXPANSION

The third-order cumulant expansion is obtained by deriving the Heisenberg equations of motion for operators up to third order and replacing the averages of fourth-order operators by lower-order ones via the rule [41,43]

$$\langle\hat{O}_1\hat{O}_2\hat{O}_3\hat{O}_4\rangle = \langle\hat{O}_1\rangle\langle\hat{O}_2\hat{O}_3\hat{O}_4\rangle + \langle\hat{O}_2\rangle\langle\hat{O}_1\hat{O}_3\hat{O}_4\rangle + \langle\hat{O}_3\rangle\langle\hat{O}_1\hat{O}_2\hat{O}_4\rangle + \langle\hat{O}_4\rangle\langle\hat{O}_1\hat{O}_2\hat{O}_3\rangle + \langle\hat{O}_1\hat{O}_2\rangle\langle\hat{O}_3\hat{O}_4\rangle + \langle\hat{O}_1\hat{O}_3\rangle\langle\hat{O}_2\hat{O}_4\rangle$$

$$+\langle\hat{O}_1\hat{O}_4\rangle\langle\hat{O}_2\hat{O}_3\rangle - 2\langle\hat{O}_1\rangle\langle\hat{O}_2\rangle\langle\hat{O}_3\hat{O}_4\rangle - 2\langle\hat{O}_1\rangle\langle\hat{O}_3\rangle\langle\hat{O}_2\hat{O}_4\rangle - 2\langle\hat{O}_1\rangle\langle\hat{O}_4\rangle\langle\hat{O}_2\hat{O}_3\rangle - 2\langle\hat{O}_2\rangle\langle\hat{O}_3\rangle\langle\hat{O}_1\hat{O}_4\rangle$$

$$-2\langle\hat{O}_2\rangle\langle\hat{O}_4\rangle\langle\hat{O}_1\hat{O}_3\rangle - 2\langle\hat{O}_3\rangle\langle\hat{O}_4\rangle\langle\hat{O}_1\hat{O}_2\rangle + 6\langle\hat{O}_1\rangle\langle\hat{O}_2\rangle\langle\hat{O}_3\rangle\langle\hat{O}_4\rangle. \tag{C1}$$

For the initial states given in Eq. (5), the nonzero expectation values at $t=0$ are those given in Eq. (B1) plus

$$\langle\hat{\sigma}_i^{ee}\hat{\sigma}_j^{ee}\hat{\sigma}_k^{ee}\rangle(t=0) = \begin{cases} 1 & \text{if atoms } i, \ j, \ \text{and } k \ \text{are excited,} \\ 0 & \text{otherwise.} \end{cases} \tag{C2}$$

Again, one can show that the decay process only couples these expectation values of populations with $\langle\hat{\sigma}_i^{eg}\hat{\sigma}_j^{ge}\rangle$ and $\langle\hat{\sigma}_i^{ee}\hat{\sigma}_j^{eg}\hat{\sigma}_k^{ge}\rangle$. Performing the expansion in Eq. (C1), one finally obtains the third-order cumulant expansion

$$\frac{d}{dt}\langle\hat{\sigma}_i^{ee}\rangle = -\Gamma_0\langle\hat{\sigma}_i^{ee}\rangle + \sum_{n\neq i}\left\{\left(iJ_{ni}-\frac{\Gamma_{ni}}{2}\right)\langle\hat{\sigma}_n^{eg}\hat{\sigma}_i^{ge}\rangle + \left(-iJ_{in}-\frac{\Gamma_{in}}{2}\right)\langle\hat{\sigma}_i^{eg}\hat{\sigma}_n^{ge}\rangle\right\}, \tag{C3a}$$

$$\frac{d}{dt}\langle\hat{\sigma}_i^{eg}\hat{\sigma}_j^{ge}\rangle = -\Gamma_0\hat{\sigma}_i^{eg}\hat{\sigma}_j^{ge} + \frac{\Gamma_{ji}}{2}\left(4\langle\hat{\sigma}_i^{ee}\hat{\sigma}_j^{ee}\rangle - \langle\hat{\sigma}_i^{ee}\rangle - \langle\hat{\sigma}_j^{ee}\rangle\right) + iJ_{ji}\left(\langle\hat{\sigma}_j^{ee}\rangle - \langle\hat{\sigma}_i^{ee}\rangle\right)$$

$$+\sum_{n\neq i,j}\left\{\left(iJ_{jn}+\frac{\Gamma_{jn}}{2}\right)\left(2\langle\hat{\sigma}_j^{ee}\hat{\sigma}_i^{eg}\hat{\sigma}_n^{ge}\rangle - \langle\hat{\sigma}_i^{eg}\hat{\sigma}_n^{ge}\rangle\right) + \left(-iJ_{ni}+\frac{\Gamma_{ni}}{2}\right)\left(2\langle\hat{\sigma}_i^{ee}\hat{\sigma}_n^{eg}\hat{\sigma}_j^{ge}\rangle - \langle\hat{\sigma}_n^{eg}\hat{\sigma}_j^{ge}\rangle\right)\right\}, \tag{C3b}$$

$$\frac{d}{dt}\langle\hat{\sigma}_i^{ee}\hat{\sigma}_j^{ee}\rangle = -2\Gamma_0\langle\hat{\sigma}_i^{ee}\hat{\sigma}_j^{ee}\rangle + \sum_{n\neq i,j}\left\{\left(iJ_{ni}-\frac{\Gamma_{ni}}{2}\right)\langle\hat{\sigma}_j^{ee}\hat{\sigma}_n^{eg}\hat{\sigma}_i^{ge}\rangle + \left(-iJ_{in}-\frac{\Gamma_{in}}{2}\right)\langle\hat{\sigma}_j^{ee}\hat{\sigma}_i^{eg}\hat{\sigma}_n^{ge}\rangle + (i\leftrightarrow j)\right\}, \tag{C3c}$$

$$\frac{d}{dt}\langle\hat{\sigma}_i^{ee}\hat{\sigma}_j^{ee}\hat{\sigma}_k^{ee}\rangle = -3\Gamma_0\langle\hat{\sigma}_i^{ee}\hat{\sigma}_j^{ee}\hat{\sigma}_k^{ee}\rangle + \sum_{n\neq i,j,k}\left\{\left(iJ_{ni}-\frac{\Gamma_{ni}}{2}\right)\left(\langle\hat{\sigma}_j^{ee}\rangle\langle\hat{\sigma}_k^{ee}\hat{\sigma}_n^{eg}\hat{\sigma}_i^{ge}\rangle + \langle\hat{\sigma}_k^{ee}\rangle\langle\hat{\sigma}_j^{ee}\hat{\sigma}_n^{eg}\hat{\sigma}_i^{ge}\rangle\right.\right.$$

$$\left.+\langle\hat{\sigma}_j^{ee}\hat{\sigma}_k^{ee}\rangle\langle\hat{\sigma}_n^{eg}\hat{\sigma}_i^{ge}\rangle - 2\langle\hat{\sigma}_j^{ee}\rangle\langle\hat{\sigma}_k^{ee}\rangle\langle\hat{\sigma}_n^{eg}\hat{\sigma}_i^{ge}\rangle\right) + \left(-iJ_{in}-\frac{\Gamma_{in}}{2}\right)\left(\langle\hat{\sigma}_j^{ee}\rangle\langle\hat{\sigma}_k^{ee}\hat{\sigma}_i^{eg}\hat{\sigma}_n^{ge}\rangle + \langle\hat{\sigma}_k^{ee}\rangle\langle\hat{\sigma}_j^{ee}\hat{\sigma}_i^{eg}\hat{\sigma}_n^{ge}\rangle\right.$$

$$\left.\left.+\langle\hat{\sigma}_j^{ee}\hat{\sigma}_k^{ee}\rangle\langle\hat{\sigma}_i^{eg}\hat{\sigma}_n^{ge}\rangle - 2\langle\hat{\sigma}_j^{ee}\rangle\langle\hat{\sigma}_k^{ee}\rangle\langle\hat{\sigma}_i^{eg}\hat{\sigma}_n^{ge}\rangle\right) + (i\leftrightarrow j) + (i\leftrightarrow k)\right\}, \tag{C3d}$$

$$\frac{d}{dt}\langle\hat{\sigma}_i^{ee}\hat{\sigma}_j^{eg}\hat{\sigma}_k^{ge}\rangle = -2\Gamma_0\langle\hat{\sigma}_i^{ee}\hat{\sigma}_j^{eg}\hat{\sigma}_k^{ge}\rangle + \left(-iJ_{ij}-\frac{\Gamma_{ij}}{2}\right)\langle\hat{\sigma}_j^{ee}\hat{\sigma}_i^{eg}\hat{\sigma}_k^{ge}\rangle + \left(iJ_{ki}-\frac{\Gamma_{ki}}{2}\right)\langle\hat{\sigma}_k^{ee}\hat{\sigma}_j^{eg}\hat{\sigma}_i^{ge}\rangle$$

$$+iJ_{kj}\left(\langle\hat{\sigma}_i^{ee}\hat{\sigma}_k^{ee}\rangle - \langle\hat{\sigma}_i^{ee}\hat{\sigma}_j^{ee}\rangle\right) + \frac{\Gamma_{kj}}{2}\left(4\langle\hat{\sigma}_i^{ee}\hat{\sigma}_j^{ee}\hat{\sigma}_k^{ee}\rangle - \langle\hat{\sigma}_i^{ee}\hat{\sigma}_j^{ee}\rangle - \langle\hat{\sigma}_i^{ee}\hat{\sigma}_k^{ee}\rangle\right)$$

$$+\sum_{n\neq i,j,k}\left\{\left(iJ_{ni}-\frac{\Gamma_{ni}}{2}\right)\left(\langle\hat{\sigma}_n^{eg}\hat{\sigma}_i^{ge}\rangle\langle\hat{\sigma}_j^{eg}\hat{\sigma}_k^{ge}\rangle + \langle\hat{\sigma}_n^{eg}\hat{\sigma}_k^{ge}\rangle\langle\hat{\sigma}_j^{eg}\hat{\sigma}_i^{ge}\rangle\right)\right.$$

$$+\left(-iJ_{in}-\frac{\Gamma_{in}}{2}\right)\left(\langle\hat{\sigma}_i^{eg}\hat{\sigma}_n^{ge}\rangle\langle\hat{\sigma}_j^{eg}\hat{\sigma}_k^{ge}\rangle + \langle\hat{\sigma}_i^{eg}\hat{\sigma}_k^{ge}\rangle\langle\hat{\sigma}_j^{eg}\hat{\sigma}_n^{ge}\rangle\right)$$

$$+\left(-iJ_{nj}+\frac{\Gamma_{nj}}{2}\right)\left(2\langle\hat{\sigma}_i^{ee}\rangle\langle\hat{\sigma}_j^{ee}\hat{\sigma}_n^{eg}\hat{\sigma}_k^{ge}\rangle + 2\langle\hat{\sigma}_j^{ee}\rangle\langle\hat{\sigma}_i^{ee}\hat{\sigma}_n^{eg}\hat{\sigma}_k^{ge}\rangle + 2\langle\hat{\sigma}_i^{ee}\hat{\sigma}_j^{ee}\rangle\langle\hat{\sigma}_n^{eg}\hat{\sigma}_k^{ge}\rangle\right)$$

$$+\left(iJ_{nj}-\frac{\Gamma_{nj}}{2}\right)\left(4\langle\hat{\sigma}_i^{ee}\rangle\langle\hat{\sigma}_j^{ee}\rangle\langle\hat{\sigma}_n^{eg}\hat{\sigma}_k^{ge}\rangle + \langle\hat{\sigma}_i^{ee}\hat{\sigma}_n^{eg}\hat{\sigma}_k^{ge}\rangle\right)$$

$$+\left(iJ_{kn}+\frac{\Gamma_{kn}}{2}\right)\left(2\langle\hat{\sigma}_i^{ee}\rangle\langle\hat{\sigma}_k^{ee}\hat{\sigma}_j^{eg}\hat{\sigma}_n^{ge}\rangle + 2\langle\hat{\sigma}_k^{ee}\rangle\langle\hat{\sigma}_i^{ee}\hat{\sigma}_j^{eg}\hat{\sigma}_n^{ge}\rangle + 2\langle\hat{\sigma}_i^{ee}\hat{\sigma}_k^{ee}\rangle\langle\hat{\sigma}_j^{eg}\hat{\sigma}_n^{ge}\rangle\right)$$

$$\left.+\left(-iJ_{kn}-\frac{\Gamma_{kn}}{2}\right)\left(4\langle\hat{\sigma}_i^{ee}\rangle\langle\hat{\sigma}_k^{ee}\rangle\langle\hat{\sigma}_j^{eg}\hat{\sigma}_n^{ge}\rangle + \langle\hat{\sigma}_i^{ee}\hat{\sigma}_j^{eg}\hat{\sigma}_n^{ge}\rangle\right)\right\}, \tag{C3e}$$

where $(a \leftrightarrow b)$ indicates that an additional term appears equal to the previous one but with indexes a and b swapped.

APPENDIX D: CRITICAL FRACTION OF EXCITED ATOMS

Let us consider an ensemble of N atoms. At the initial time, N_{exc} of them are excited, while the remaining $N_{\text{de}} = N - N_{\text{exc}}$ are deexcited (see Sec. IV B). We label as $\mathcal{E}$ and $\mathcal{D}$ the set of excited and deexcited atoms, respectively. We consider incoherently excited arrays, such that $\langle \hat{\sigma}_i^{ee} \rangle_0 = 1$ if $i \in \mathcal{E}$ and zero otherwise, and $\langle \hat{\sigma}_i^{ee} \hat{\sigma}_j \rangle_0 = 1$ if $i, j \in \mathcal{E}$ and zero otherwise. The derivative of the total emission rate for any configuration, given in Eq. (9), can be expressed as

$$\dot{\gamma}_{\text{tot},0} = -\sum_i \frac{d^2}{dt^2} \langle \hat{\sigma}_i^{ee} \rangle_0, \tag{D1}$$

$$-\frac{d^2}{dt^2} \langle \hat{\sigma}_i^{ee} \rangle_0 = -\Gamma_0^2 \langle \hat{\sigma}_i^{ee} \rangle_0 + \sum_{j \neq i} \frac{\Gamma_{ij} \Gamma_{ji}}{2} \left(4 \langle \hat{\sigma}_i^{ee} \hat{\sigma}_j^{ee} \rangle_0 - \langle \hat{\sigma}_i^{ee} \rangle_0 + \langle \hat{\sigma}_j^{ee} \rangle_0 \right). \tag{D2}$$

If all atoms are excited, one simply obtains $-\frac{d^2}{dt^2} \langle \hat{\sigma}_i^{ee} \rangle_0 = -\Gamma_0^2 + \sum_{j \neq i} \Gamma_{ij} \Gamma_{ji}$. In the presence of deexcited atoms, one gets instead

$$-\frac{d^2}{dt^2} \langle \hat{\sigma}_{i \in \mathcal{E}}^{ee} \rangle_0 = -\Gamma_0^2 + \sum_{j \neq i} \Gamma_{ij} \Gamma_{ji} - 1.5 \sum_{j \in D} \Gamma_{ij} \Gamma_{ji}, \tag{D3}$$

$$-\frac{d^2}{dt^2} \langle \hat{\sigma}_{i \in \mathcal{D}}^{ee} \rangle_0 = -0.5 \sum_{j \in \mathcal{E}} \Gamma_{ij} \Gamma_{ji}. \tag{D4}$$

Plugging these expressions into Eq. (D1), we obtain

$$\dot{\gamma}_{\text{tot},0} = -\Gamma_0^2 N_{\text{exc}} + \sum_i \sum_{j \neq i} \Gamma_{ij} \Gamma_{ji} - 3 \sum_{i \in \mathcal{D}} \sum_{j \neq i} \Gamma_{ij} \Gamma_{ji} + 2 \sum_{i \in \mathcal{D}} \sum_{j \in D, j \neq i} \Gamma_{ij} \Gamma_{ji}. \tag{D5}$$

We further average over all possible configurations of N_{de} deexcited atoms. We label the deexcited atoms with indexes α_1 to $\alpha_{N_{\text{de}}}$, each of them taking values from 1 to N. Noting that no two indexes can be equal, the total number of permutations is $N!/(N - N_{\text{de}})!$. Then, the average derivative of the total decay rate can be written as

$$\bar{\dot{\gamma}}_{\text{tot},0} = -\Gamma_0^2 N_{\text{exc}} + \sum_i \sum_{j \neq i} \Gamma_{ij} \Gamma_{ji} - 3 \Sigma_1 + 2 \Sigma_2, \tag{D6}$$

where Σ_1 and Σ_2 are

$$\Sigma_1 = \frac{(N - N_{\text{de}})!}{N!} \sum_{\alpha_1} \sum_{\alpha_2 \neq \alpha_1} \cdots \sum_{\alpha_{N_{de}} \neq \alpha_1, \ldots, \alpha_{N_{de}-1}} \sum_{i \in \mathcal{D}} \sum_{j \neq i} \Gamma_{ij} \Gamma_{ji}$$

$$= \frac{(N - N_{\text{de}})!}{N!} \sum_{\alpha_1} \sum_{\alpha_2 \neq \alpha_1} \cdots \sum_{\alpha_{N_{de}} \neq \alpha_1, \ldots, \alpha_{N_{de}-1}} \left(\sum_{j \neq \alpha_1} \Gamma_{\alpha_1 j} \Gamma_{j \alpha_1} + \cdots + \sum_{j \neq \alpha_{N_{de}}} \Gamma_{\alpha_{N_{de}} j} \Gamma_{j \alpha_{N_{de}}} \right)$$

$$= N_{\text{de}} \frac{(N - N_{\text{de}})!}{N!} \sum_{\alpha_1} \sum_{j \neq \alpha_1} \Gamma_{\alpha_1 j} \Gamma_{j \alpha_1} \left(\sum_{\alpha_2 \neq \alpha_1} \cdots \sum_{\alpha_{N_{de}} \neq \alpha_1, \ldots, \alpha_{N_{de}-1}} \right)$$

$$= \frac{N_{\text{de}}}{N} \sum_i \sum_{j \neq i} \Gamma_{ij} \Gamma_{ji}, \tag{D7}$$

$$\Sigma_2 = \frac{(N - N_{\text{de}})!}{N!} \sum_{\alpha_1} \sum_{\alpha_2 \neq \alpha_1} \cdots \sum_{\alpha_{N_{de}} \neq \alpha_1, \ldots, \alpha_{N_{de}-1}} \sum_{i \in \mathcal{D}} \sum_{j \in \mathcal{D}, j \neq i} \Gamma_{ij} \Gamma_{ji}$$

$$= \frac{(N - N_{\text{de}})!}{N!} \sum_{\alpha_1} \sum_{\alpha_2 \neq \alpha_1} \cdots \sum_{\alpha_{N_{de}} \neq \alpha_1, \ldots, \alpha_{N_{de}-1}} \left(\Gamma_{\alpha_1 \alpha_2} \Gamma_{\alpha_2 \alpha_1} + \cdots + \Gamma_{\alpha_1 \alpha_{N_{de}}} \Gamma_{\alpha_{N_{de}} \alpha_1} + \Gamma_{\alpha_2 \alpha_3} \Gamma_{\alpha_3 \alpha_2} + \cdots \right)$$

$$= N_{\text{de}}(N_{\text{de}} - 1) \frac{(N - N_{\text{de}})!}{N!} \sum_{\alpha_1} \sum_{\alpha_2 \neq \alpha_1} \Gamma_{\alpha_1 \alpha_2} \Gamma_{\alpha_2 \alpha_1} \left(\sum_{\alpha_3 \neq \alpha_1, \alpha_2} \cdots \sum_{\alpha_{N_{de}} \neq \alpha_1, \ldots, \alpha_{N_{de}-1}} \right)$$

$$= \frac{N_{\text{de}}(N_{\text{de}} - 1)}{N(N - 1)} \sum_i \sum_{j \neq i} \Gamma_{ij} \Gamma_{ji}, \tag{D8}$$

and they finally result in Eq. (11) of the main text.

APPENDIX E: CRITICAL FILLING FRACTION

Let us consider an array with N lattice positions, N_{filled} of which are occupied and $N_{\text{hol}} = N - N_{\text{filled}}$ are empty (see Sec. IV C). Labeling $\mathcal{F}$ and $\mathcal{H}$ as the set of filled and empty lattice sites, we can compute the derivative of the total emission rate in a similar manner as in Appendix D. Now, the second-order derivatives of the population in lattice site i read

$$-\frac{d^2}{dt^2}\langle\hat{\sigma}^{ee}_{i\in\mathcal{F}}\rangle_0 = -\Gamma_0^2 + \sum_{j\in\mathcal{F},j\neq i}\Gamma_{ij}\Gamma_{ji}, \tag{E1}$$

$$-\frac{d^2}{dt^2}\langle\hat{\sigma}^{ee}_{i\in\mathcal{H}}\rangle_0 = 0. \tag{E2}$$

Note that the population at the lattice site of a missing atom is always zero, and so is its second derivative. The population in a filled lattice site, on the other hand, is equal to that of an alternative, fully inverted system containing only N_{filled} atoms at the occupied positions.

Then, $\dot{\bar{\gamma}}_{\text{tot},0}$ can be written as

$$\bar{\dot{\gamma}}_{\text{tot},0} = -\Gamma_0^2 N_{\text{filled}} + \sum_{i\in\mathcal{F}}\sum_{j\in\mathcal{F},j\neq i}\Gamma_{ij}\Gamma_{ji}$$

$$= -\Gamma_0^2 N_{\text{filled}} + \sum_i\sum_{j\neq i}\Gamma_{ij}\Gamma_{ji}$$

$$- 2\sum_{i\in\mathcal{H}}\sum_{j\neq i}\Gamma_{ij}\Gamma_{ji} + \sum_{i\in\mathcal{H}}\sum_{j\in H,j\neq i}\Gamma_{ij}\Gamma_{ji}, \tag{E3}$$

which takes the same form as Eq. (D5) but with different prefactors. Using Eqs. (D7) and (D8), one readily finds the average derivative of the total emission rate, given in Eq. (13) of the main text.

[1] R. H. Dicke, Coherence in spontaneous radiation processes, Phys. Rev. **93**, 99 (1954).

[2] M. Gross and S. Haroche, Superradiance: An essay on the theory of collective spontaneous emission, Phys. Rep. **93**, 301 (1982).

[3] N. E. Rehler and J. H. Eberly, Superradiance, Phys. Rev. A **3**, 1735 (1971).

[4] G. Banfi and R. Bonifacio, Superfluorescence and cooperative frequency shift, Phys. Rev. A **12**, 2068 (1975).

[5] S. Fuchs, A. Vukics, and S. Y. Buhmann, Superradiance from nonideal initial states: A quantum trajectory approach, Phys. Rev. A **103**, 043712 (2021).

[6] N. Shammah, N. Lambert, F. Nori, and S. De Liberato, Superradiance with local phase-breaking effects, Phys. Rev. A **96**, 023863 (2017).

[7] D. Malz, R. Trivedi, and J. I. Cirac, Large-n limit of dicke superradiance, Phys. Rev. A **106**, 013716 (2022).

[8] B. Lemberger and K. Mølmer, Radiation eigenmodes of dicke superradiance, Phys. Rev. A **103**, 033713 (2021).

[9] S. Inouye, A. P. Chikkatur, D. M. Stamper-Kurn, J. Stenger, D. E. Pritchard, and W. Ketterle, Superradiant rayleigh scattering from a bose-einstein condensate, Science **285**, 571 (1999).

[10] T. Wang, S. F. Yelin, R. Côté, E. E. Eyler, S. M. Farooqi, P. L. Gould, M. Koštrun, D. Tong, and D. Vrinceanu, Superradiance in ultracold Rydberg gases, Phys. Rev. A **75**, 033802 (2007).

[11] D. D. Grimes, S. L. Coy, T. J. Barnum, Y. Zhou, S. F. Yelin, and R. W. Field, Direct single-shot observation of millimeter-wave superradiance in Rydberg-Rydberg transitions, Phys. Rev. A **95**, 043818 (2017).

[12] Y. Kaluzny, P. Goy, M. Gross, J. M. Raimond, and S. Haroche, Observation of Self-Induced Rabi Oscillations in Two-Level Atoms Excited Inside a Resonant Cavity: The Ringing Regime of Superradiance, Phys. Rev. Lett. **51**, 1175 (1983).

[13] M. O. Araújo, I. Krešić, R. Kaiser, and W. Guerin, Superradiance in a Large and Dilute Cloud of Cold Atoms in the Linear-Optics Regime, Phys. Rev. Lett. **117**, 073002 (2016).

[14] L. Chen, P. Wang, Z. Meng, L. Huang, H. Cai, D.-W. Wang, S.-Y. Zhu, and J. Zhang, Experimental Observation of One-Dimensional Superradiance Lattices in Ultracold Atoms, Phys. Rev. Lett. **120**, 193601 (2018).

[15] A. Goban, C.-L. Hung, J. D. Hood, S.-P. Yu, J. A. Muniz, O. Painter, and H. J. Kimble, Superradiance for Atoms Trapped along a Photonic Crystal Waveguide, Phys. Rev. Lett. **115**, 063601 (2015).

[16] M. Scheibner, T. Schmidt, L. Worschech, A. Forchel, G. Bacher, T. Passow, and D. Hommel, Superradiance of quantum dots, Nat. Phys. **3**, 106 (2007).

[17] G. Rainò, M. A. Becker, M. I. Bodnarchuk, R. F. Mahrt, M. V. Kovalenko, and T. Stöferle, Superfluorescence from lead halide perovskite quantum dot superlattices, Nature (London) **563**, 671 (2018).

[18] C. Bradac, M. T. Johnsson, M. v. Breugel, B. Q. Baragiola, R. Martin, M. L. Juan, G. K. Brennen, and T. Volz, Room-temperature spontaneous superradiance from single diamond nanocrystals, Nat. Commun. **8**, 1205 (2017).

[19] G. Haider, K. Sampathkumar, T. Verhagen, L. Nádvorník, F. J. Sonia, V. Valeš, J. Sýkora, P. Kapusta, P. Němec, M. Hof, O. Frank, Y.-F. Chen, J. Vejpravová, and M. Kalbáč, Superradiant emission from coherent excitons in van der waals heterostructures, Adv. Funct. Mater. **31**, 2102196 (2021).

[20] A. Asenjo-Garcia, M. Moreno-Cardoner, A. Albrecht, H. J. Kimble, and D. E. Chang, Exponential Improvement in Photon Storage Fidelities Using Subradiance and "Selective Radiance" in Atomic Arrays, Phys. Rev. X **7**, 031024 (2017).

[21] J. Rui, D. Wei, A. Rubio-Abadal, S. Hollerith, J. Zeiher, D. M. Stamper-Kurn, C. Gross, and I. Bloch, A subradiant optical mirror formed by a single structured atomic layer, Nature (London) **583**, 369 (2020).

[22] E. Shahmoon, D. S. Wild, M. D. Lukin, and S. F. Yelin, Cooperative Resonances in Light Scattering from Two-Dimensional Atomic Arrays, Phys. Rev. Lett. **118**, 113601 (2017).

[23] R. J. Bettles, S. A. Gardiner, and C. S. Adams, Enhanced Optical Cross Section via Collective Coupling of Atomic Dipoles in a 2D Array, Phys. Rev. Lett. **116**, 103602 (2016).

[24] O. Rubies-Bigorda, V. Walther, T. L. Patti, and S. F. Yelin, Photon control and coherent interactions via lattice dark states in atomic arrays, Phys. Rev. Res. **4**, 013110 (2022).

[25] K. E. Ballantine and J. Ruostekoski, Quantum single-photon control, storage, and entanglement generation with planar atomic arrays, PRX Quantum **2**, 040362 (2021).

[26] M. Moreno-Cardoner, R. Holzinger, and H. Ritsch, Efficient nano-photonic antennas based on dark states in quantum emitter rings, Opt. Express **30**, 10779 (2022).

[27] J. Perczel, J. Borregaard, D. E. Chang, H. Pichler, S. F. Yelin, P. Zoller, and M. D. Lukin, Topological Quantum Optics in Two-Dimensional Atomic Arrays, Phys. Rev. Lett. **119**, 023603 (2017).

[28] E. Shahmoon, M. D. Lukin, and S. F. Yelin, Quantum optomechanics of a two-dimensional atomic array, Phys. Rev. A **101**, 063833 (2020).

[29] M. Moreno-Cardoner, D. Goncalves, and D. E. Chang, Quantum Nonlinear Optics Based on Two-Dimensional Rydberg Atom Arrays, Phys. Rev. Lett. **127**, 263602 (2021).

[30] S. Buckley-Bonanno, S. Ostermann, O. Rubies-Bigorda, T. L. Patti, and S. F. Yelin, Optimized geometries for cooperative photon storage in an impurity coupled to a two-dimensional atomic array, Phys. Rev. A **106**, 053706 (2022).

[31] L. Zhang, V. Walther, K. Mølmer, and T. Pohl, Photon-photon interactions in Rydberg-atom arrays, Quantum **6**, 674 (2022).

[32] J. P. Clemens, L. Horvath, B. C. Sanders, and H. J. Carmichael, Collective spontaneous emission from a line of atoms, Phys. Rev. A **68**, 023809 (2003).

[33] H. Carmichael and K. Kim, A quantum trajectory unraveling of the superradiance master equation, Opt. Commun. **179**, 417 (2000).

[34] S. J. Masson, I. Ferrier-Barbut, L. A. Orozco, A. Browaeys, and A. Asenjo-Garcia, Many-Body Signatures of Collective Decay in Atomic Chains, Phys. Rev. Lett. **125**, 263601 (2020).

[35] S. J. Masson and A. Asenjo-Garcia, Universality of dicke superradiance in arrays of quantum emitters, Nat. Commun. **13**, 2285 (2022).

[36] E. Sierra, S. J. Masson, and A. Asenjo-Garcia, Dicke superradiance in ordered lattices: Dimensionality matters, Phys. Rev. Res. **4**, 023207 (2022).

[37] F. Robicheaux, Theoretical study of early-time superradiance for atom clouds and arrays, Phys. Rev. A **104**, 063706 (2021).

[38] G.-D. Lin and S. F. Yelin, Superradiance: An integrated approach to cooperative effects in various systems, in *Advances in Atomic, Molecular, and Optical Physics*, edited by P. Berman, E. Arimondo, and C. Lin (Academic, 2012), Vol. 61, Chap. 6, pp. 295–329.

[39] O. Rubies-Bigorda and S. F. Yelin, Superradiance and subradiance in inverted atomic arrays, Phys. Rev. A **106**, 053717 (2022).

[40] H. Ma, O. Rubies-Bigorda, and S. F. Yelin, Superradiance and subradiance in a gas of two-level atoms, arXiv:2205.15255.

[41] R. Kubo, Generalized cumulant expansion method, J. Phys. Soc. Jpn. **17**, 1100 (1962).

[42] S. Krämer and H. Ritsch, Generalized mean-field approach to simulate the dynamics of large open spin ensembles with long range interactions, Europhys. J. D **69**, 282 (2015).

[43] D. Plankensteiner, C. Hotter, and H. Ritsch, QuantumCumulants.jl: A Julia framework for generalized mean-field equations in open quantum systems, Quantum **6**, 617 (2022).

[44] F. Robicheaux and D. A. Suresh, Beyond lowest order mean-field theory for light interacting with atom arrays, Phys. Rev. A **104**, 023702 (2021).

[45] R. Dum, P. Zoller, and H. Ritsch, Monte Carlo simulation of the atomic master equation for spontaneous emission, Phys. Rev. A **45**, 4879 (1992).

[46] K. Mølmer, Y. Castin, and J. Dalibard, Monte Carlo wave-function method in quantum optics, J. Opt. Soc. Am. B **10**, 524 (1993).

[47] R. H. Lehmberg, Radiation from an *n*-atom system. i. general formalism, Phys. Rev. A **2**, 883 (1970).

[48] R. H. Lehmberg, Radiation from an *n*-atom system. ii. spontaneous emission from a pair of atoms, Phys. Rev. A **2**, 889 (1970).

[49] O. Rubies-Bigorda, S. Ostermann, and S. F. Yelin, Generating multi-excitation subradiant states in incoherently excited atomic arrays, arXiv:2209.00034.

[50] X. Huang, W. Yuan, A. Holman, M. Kwon, S. J. Masson, R. Gutierrez-Jauregui, A. Asenjo-Garcia, S. Will, and N. Yu, Metasurface holographic optical traps for ultracold atoms, arXiv:2210.07425.

[51] T. I. Andersen, R. J. Gelly, G. Scuri, B. L. Dwyer, D. S. Wild, R. Bekenstein, A. Sushko, J. Sung, Y. Zhou, A. A. Zibrov, X. Liu, A. Y. Joe, K. Watanabe, T. Taniguchi, S. F. Yelin, P. Kim, H. Park, and M. D. Lukin, Spatial light modulation at the nanosecond scale with an atomically thin reflector, Nat. Commun. **13**, 3431 (2022).

[52] F. Dimer, B. Estienne, A. S. Parkins, and H. J. Carmichael, Proposed realization of the dicke-model quantum phase transition in an optical cavity qed system, Phys. Rev. A **75**, 013804 (2007).

[53] K. Baumann, C. Guerlin, F. Brennecke, and T. Esslinger, Dicke quantum phase transition with a superfluid gas in an optical cavity, Nature (London) **464**, 1301 (2010).

[54] J. Klinder, H. Keßler, M. Wolke, L. Mathey, and A. Hemmerich, Dynamical phase transition in the open dicke model, Proc. Natl. Acad. Sci. USA **112**, 3290 (2015).

[55] G. Ferioli, A. Glicenstein, I. Ferrier-Barbut, and A. Browaeys, Observation of a non-equilibrium superradiant phase transition in free space, arXiv:2207.10361.

[56] W. C. Chew, *Waves and Fields in Inhomogeneous Media (Electromagnetic Waves)* (IEEE Computer Society, 1995).

[57] L. Novotny and B. Hecht, *Principles of Nano-Optics* (Cambridge University Press, 2006).